

Supporting Information

***In situ* Active Site for CO Activation in Fe-catalyzed Fischer-Tropsch Synthesis from Machine Learning**

Qian-Yu Liu, Cheng Shang*, Zhi-Pan Liu*

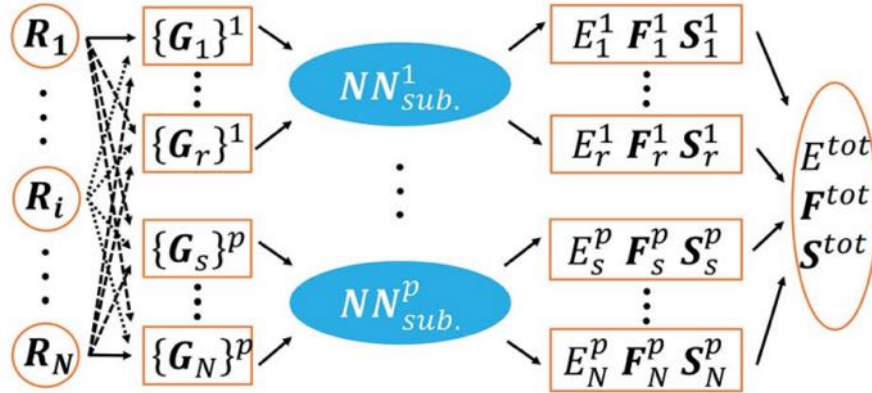
Collaborative Innovation Center of Chemistry for Energy Material, Shanghai Key Laboratory of Molecular Catalysis and Innovative Materials, Key Laboratory of Computational Physical Science, Department of Chemistry, Fudan University, Shanghai 200433, China

Table of Contents

- 1. Methods: Construction of Fe-C-H-O quaternary G-NN potential**
- 2. Benchmark of G-NN potential against DFT calculations**
- 3. Calculations of carbon chemical potential (μ_C)**
- 4. FeC_x bulk phase**
- 5. FeC_x surfaces**
- 6. Adsorption sites for H/CO**
- 7. H and C diffusion on the surface from molecular dynamics**
- 8. Other CO activation pathways and CH_x diffusion pathway**

1. Methods: Construction of Fe-C-H-O quaternary G-NN potential

1.1 Architecture of neural network potential



Scheme S1. Scheme for the HDNN architecture. The subscripts i and N represent atom indices and total number of atoms in a structure. The input of a NN is a set of structural descriptors $\{\mathbf{G}_i\}$ constructed from Cartesian coordinates $\{\mathbf{R}\}$ of a structure, and the outputs are the atomic properties $\{E_i, \mathbf{F}_i, \mathbf{S}_i\}$, i.e. energy, forces and stresses. The overall properties E^{tot} , \mathbf{F}^{tot} , and \mathbf{S}^{tot} , can be calculated from the individual atomic contributions.

In this work, we utilized the high dimensional neural network (HDNN) scheme to construct the NN potential¹⁻⁴. The NN architecture is schematically shown in Scheme S1. In Eq. 1, the total energy E^{tot} can be decomposed and written as a linear combination of atomic energy E_i , which is the output of the standard neural network. The input nodes are a set of geometry-based structural descriptors, $\{\mathbf{G}_i\}$.

$$E^{tot} = \sum_i E_i \quad (1)$$

The atomic force can be analytically derived according to Eq. 2, where the force component $F_{k,\alpha}$, $\alpha=x, y$ or z , acting on the atom k is the derivative of the total energy with respect to its coordinate $R_{k,\alpha}$. By combining with Eq. 1, the force component can be further related to the derivatives of the atomic energy with respect to j^{th} structural descriptors of atom i , $G_{j,i}$:

$$F_{k,\alpha} = -\frac{\partial E^{tot}}{\partial R_{k,\alpha}} = -\sum_{i,j} \frac{\partial E_i}{\partial G_{j,i}} \frac{\partial G_{j,i}}{\partial R_{k,\alpha}} \quad (2)$$

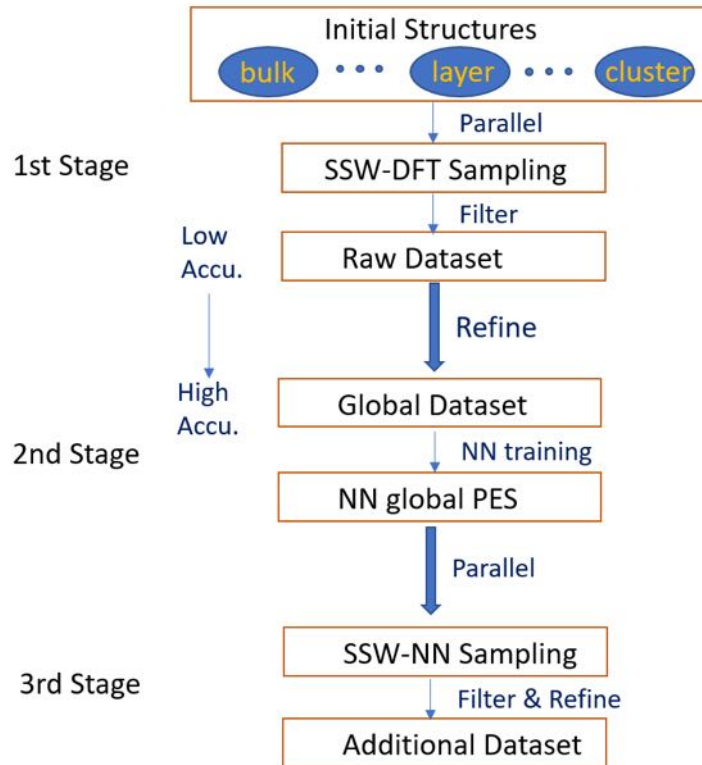
Similarly, the static stress tensor matrix element $\sigma_{\alpha\beta}$ can be analytically derived as:

$$\sigma_{\alpha\beta} = -\frac{1}{V} \sum_{i,j,d} \frac{(\mathbf{r}_d)_\alpha (\mathbf{r}_d)_\beta}{r_d} \frac{\partial E_i}{\partial G_{j,i}} \frac{\partial G_{j,i}}{\partial r_d} \quad (3)$$

where \mathbf{r}_d and r_d are the distance vector constituting of $G_{j,i}$ and its module, respectively, and V is the volume of the structure.

1.2 Construction of global dataset using SSW-NN

Undoubtedly, the dataset used for training the NN determines largely the quality of the potential energy surface (PES) of G-NN. Our previous works have shown that the stochastic surface walking (SSW) global optimization⁵⁻⁷ can be used to fast generate a global dataset, which incorporates



Scheme S2. Procedure for the generation of the global training dataset by SSW global optimization. In the first stage, the SSW sampling is typically performed by low accuracy DFT calculations. In the second stage, the global dataset is first refined with high accuracy DFT setups, and then a NN training is performed based on the accurate global dataset. In the third stage, an additional dataset is generated by SSW sampling utilizing the previously obtained NN PES, and is fed into the global dataset. A new cycle of NN training then starts based on the new global dataset (back to stage 2).

different structural patterns on the global PES. The SSW PES search is fully automated and does not need a priori knowledge on the system, such as the structure motif (e.g., bonding patterns, symmetry) of materials. The brief description of the Fe-C-H-O global dataset in this work is detailed in Table S1, and the dataset can be openly downloaded from http://www.lasphub.com/supportings/Trainfile_FeCHO.tar.gz.

In brief, the SSW-NN method involves three stages for constructing the global dataset, as described in the following.

- (i) **The first stage** constructs a raw dataset, which contains the most common atomic environment and serves as the training dataset for building an initial NN PES. This is done by performing density functional theory (DFT) SSW global optimization in a massively parallel way. The DFT calculation is typically with low accuracy setups and restricted to small unit cells to speed up the SSW search. By collecting and screening the structures from the SSW trajectories, a raw dataset is finally obtained. The low accuracy calculations use 300 eV kinetics energy cutoff and 15 \AA^{-1} k -point auto-mesh (15 \AA^{-1} auto-mesh means the first Brillouin zone k -point sampling adopted the Monkhorst-Pack scheme with an automated mesh determined by 15 times the reciprocal lattice vectors).

- (ii) **The second stage** trains an NN global PES. This is done by first refining the dataset using first principles calculation with high accuracy setups, followed by the NN training on the accurate global dataset. The high accuracy calculation for producing the dataset use 450 eV kinetics energy cutoff and 25 \AA^{-1} k -point auto-mesh. The NN architecture applied in this stage utilizes a small set of structural descriptors and a small network size.
- (iii) **The third stage** iteratively expands the global dataset. It targets to increase the predictive power of NN PES by incorporating more structural patterns into the dataset. This is done by carrying out SSW PES search using the NN PES obtained in the second stage, starting from a variety of initial structures. These initial structures are often randomly configurated and also include large systems with many atoms per unit cell. The structures from all SSW trajectories are collected and filtered to generate the additional dataset. This new dataset is then fed to the global dataset (back to stage 2) to start a new cycle of NN training.

Table S1. Structure information of the global EPS data set for G-NN potential training. The listed data is the number of structures in the data set, as distinguished by the chemical formula, the number of atoms per cell (N_{atm}) and the type of structure, including cluster (N_{cls}), layer (N_{lay}) and bulk (N_{bul}). The total numbers of the structure (N_{tot}) are also summarized.

Species	N_{atm}	N_{cls}	N_{lay}	N_{bul}	N_{tot}
Fe4	4	0	0	6	6
Fe16	16	16	82	294	392
Fe32	32	0	27	6	33
O1-Fe3	4	0	0	1	1
O1-Fe15	16	1	2	10	13
O2-Fe11	13	0	1	0	1
O2-Fe14	16	0	4	10	14
O2-Fe30	32	0	2	0	2
C1-Fe12	13	0	39	0	39
C1-Fe18	19	0	81	240	321
C1-Fe31	32	0	122	1	123
C1-O1-Fe11	13	0	2	0	2
C1-O1-Fe17	19	0	4	8	12
C1-O1-Fe30	32	0	2	0	2
C1-O2-Fe9	12	0	1	0	1
C1-O2-Fe16	19	0	2	6	8
C1-O2-Fe29	32	0	1	0	1
C2-Fe10	12	0	53	0	53
C2-Fe17	19	0	0	30	30
C2-Fe25	27	0	0	1	1
C2-Fe29	31	0	0	10	10
C2-Fe36	38	0	21	0	21
C2-O1-Fe9	12	0	3	0	3
C2-O1-Fe16	19	0	0	1	1
C2-O2-Fe8	12	0	1	0	1

C2-O2-Fe15	19	0	0	1	1
C2-O2-Fe34	38	0	1	0	1
C3-Fe16	19	5	0	0	5
C3-O1-Fe8	12	0	0	1	1
C3-O2-Fe7	12	0	0	2	2
C4-Fe8	12	0	0	182	182
C4-Fe12	16	0	0	52	52
C4-Fe25	29	0	0	1	1
C4-O1-Fe7	12	0	0	3	3
C4-O2-Fe6	12	0	0	2	2
C5-Fe14	19	0	10	4	14
C5-O1-Fe12	18	0	0	2	2
C5-O1-Fe13	19	0	1	0	1
C5-O1-Fe14	20	0	0	3	3
C5-O1-Fe23	29	0	1	0	1
C5-O2-Fe11	18	0	2	1	3
C5-O2-Fe13	20	0	2	0	2
C5-O2-Fe14	21	0	1	1	2
C5-O2-Fe22	29	0	0	3	3
C5-O2-Fe24	31	0	1	0	1
C6-Fe10	16	0	1	8	9
C6-Fe12	18	0	117	104	221
C6-Fe14	20	0	109	119	228
C6-Fe15	21	0	77	123	200
C6-Fe23	29	0	89	197	286
C6-Fe24	30	0	0	137	137
C6-Fe25	31	0	120	260	380
C6-O1-Fe9	16	0	0	2	2
C6-O1-Fe11	18	0	2	4	6
C6-O1-Fe13	20	0	2	1	3
C6-O1-Fe14	21	0	3	2	5
C6-O1-Fe22	29	0	1	2	3
C6-O1-Fe24	31	0	1	2	3
C6-O2-Fe10	18	0	3	3	6
C6-O2-Fe12	20	0	4	2	6
C6-O2-Fe13	21	0	1	3	4
C6-O2-Fe21	29	0	1	8	9
C6-O2-Fe23	31	0	2	3	5
C7-Fe16	23	0	0	24	24
C7-O2-Fe11	20	0	0	1	1
C7-O2-Fe15	24	1	0	0	1
C8	8	0	17	289	306
C8-Fe12	20	0	8	36	44
C8-Fe16	24	3	0	33	36

C8-Fe20	28	0	0	52	52
C9-Fe15	24	0	15	30	45
C9-O1-Fe14	24	0	1	0	1
C9-O2-Fe9	20	0	0	1	1
C9-O2-Fe12	23	0	0	1	1
C10-Fe10	20	0	21	40	61
C10-Fe13	23	0	0	17	17
C10-Fe22	32	0	0	86	86
C10-Fe27	37	0	9	0	9
C10-Fe28	38	0	3	1	4
C10-Fe30	40	0	10	8	18
C10-O1-Fe9	20	0	1	0	1
C10-O2-Fe8	20	0	1	1	2
C10-O2-Fe16	28	0	0	1	1
C11-Fe28	39	0	10	3	13
C11-O1-Fe27	39	0	1	0	1
C11-O1-Fe30	42	0	179	17	196
C11-O2-Fe27	40	0	1	0	1
C11-O2-Fe29	42	0	1	0	1
C12-Fe16	28	0	20	61	81
C12-Fe20	32	0	0	64	64
C12-Fe24	36	0	25	0	25
C12-Fe26	38	0	8	1	9
C12-Fe27	39	0	3	1	4
C12-Fe28	40	0	75	324	399
C12-Fe30	42	0	27	0	27
C12-Fe46	58	0	23	0	23
C12-Fe50	62	0	19	0	19
C12-O1-Fe27	40	0	0	1	1
C12-O2-Fe14	28	0	1	1	2
C12-O2-Fe26	40	0	1	1	2
C12-O2-Fe28	42	0	136	0	136
C13-O1-Fe28	42	0	51	0	51
C13-O1-Fe30	44	0	44	1	45
C14-O1-Fe29	44	0	49	0	49
C15-O2-Fe25	42	0	2	0	2
C16-Fe24	40	0	0	107	107
C16-Fe26	42	0	111	0	111
C16-O2-Fe24	42	0	1	0	1
C17-Fe41	58	0	97	1	98
C18-O2-Fe16	36	0	2	0	2
C19-Fe17	36	0	122	1	123
C19-O1-Fe16	36	0	1	0	1
C19-O2-Fe15	36	0	2	0	2

C22-Fe55	77	0	1	1	2
C22-Fe56	78	0	3	0	3
C24-Fe51	75	0	3	1	4
C24-Fe52	76	0	4	1	5
C24-Fe53	77	0	3	1	4
C24-Fe54	78	0	3	2	5
C25-Fe11	36	0	49	1	50
C28-Fe16	44	0	33	3	36
C30-O2-Fe72	104	0	23	0	23
C30-O2-Fe74	106	0	61	0	61
C32-Fe74	106	0	18	0	18
C32-O2-Fe74	108	0	90	0	90
C38-Fe16	54	0	23	0	23
C39-Fe120	159	0	3	0	3
C40-Fe16	56	0	23	0	23
C41-Fe120	161	0	12	0	12
C42-Fe120	162	0	20	0	20
C44-Fe16	60	0	50	1	51
C47-Fe96	143	0	85	0	85
C47-Fe112	159	0	20	0	20
C47-Fe120	167	0	11	0	11
C49-Fe96	145	0	21	0	21
C49-Fe112	161	0	27	0	27
C49-Fe120	169	0	5	0	5
C49-O1-Fe120	170	0	170	0	170
C50-Fe96	146	0	16	0	16
C50-Fe112	162	0	16	0	16
C50-Fe120	170	0	8	0	8
C60-O4-Fe144	208	0	3	0	3
C60-O4-Fe148	212	0	3	0	3
C64-Fe148	212	0	1	0	1
C64-O4-Fe148	216	0	4	0	4
H1-Fe15	16	0	0	23	23
H1-Fe16	17	0	0	1	1
H1-Fe23	24	0	5	0	5
H1-Fe26	27	0	10	0	10
H1-Fe27	28	0	6	0	6
H1-Fe31	32	0	0	3	3
H1-O2-Fe13	16	0	0	1	1
H1-C1-Fe30	32	0	52	1	53
H1-C5-Fe18	24	0	0	7	7
H1-C6-O2-Fe15	24	0	1	0	1
H1-C7-O1-Fe15	24	0	2	0	2
H1-C7-O2-Fe10	20	0	3	0	3

H1-C8-Fe11	20	0	67	2	69
H1-C8-Fe15	24	0	96	2	98
H1-C8-O1-Fe10	20	0	4	0	4
H1-C8-O1-Fe14	24	0	1	0	1
H1-C8-O2-Fe9	20	0	7	0	7
H1-C9-Fe10	20	0	441	56	497
H1-C9-O1-Fe9	20	0	4	0	4
H1-C9-O2-Fe8	20	0	7	0	7
H1-C9-O2-Fe16	28	0	2	0	2
H1-C10-O1-Fe16	28	0	3	0	3
H1-C10-O2-Fe15	28	0	6	0	6
H1-C11-Fe16	28	0	234	44	278
H1-C11-O1-Fe15	28	0	1	1	2
H1-C11-O2-Fe14	28	0	3	2	5
H1-C11-O2-Fe28	42	0	271	2	273
H1-C12-O1-Fe28	42	0	95	0	95
H1-C41-Fe120	162	0	1	0	1
H1-C42-Fe120	163	0	13	0	13
H1-C49-Fe96	146	0	17	0	17
H1-C49-Fe112	162	0	21	0	21
H1-C49-Fe120	170	0	1	0	1
H1-C49-O1-Fe120	171	0	198	0	198
H1-C50-Fe96	147	0	3	0	3
H1-C50-Fe112	163	0	5	0	5
H1-C50-Fe120	171	0	9	0	9
H2-Fe14	16	0	5	42	47
H2-Fe16	18	0	88	91	179
H2-Fe21	23	0	0	10	10
H2-Fe22	24	0	1	0	1
H2-Fe27	29	1	1	5	7
H2-Fe28	30	0	5	0	5
H2-Fe30	32	1	0	2	3
H2-O1-Fe13	16	0	0	2	2
H2-O1-Fe15	18	0	6	3	9
H2-O2-Fe14	18	0	0	4	4
H2-C1-O2-Fe12	17	0	15	1	16
H2-C1-O2-Fe16	21	0	10	0	10
H2-C1-O2-Fe20	25	0	4	0	4
H2-C1-O2-Fe36	41	0	11	0	11
H2-C1-O3-Fe36	42	0	3	0	3
H2-C2-Fe18	22	0	0	16	16
H2-C2-O2-Fe16	22	0	0	2	2
H2-C2-O3-Fe26	33	0	1	0	1
H2-C2-O3-Fe27	34	0	7	0	7

H2-C3-Fe17	22	0	0	17	17
H2-C3-O1-Fe23	29	0	1	0	1
H2-C3-O2-Fe22	29	0	0	4	4
H2-C3-O2-Fe26	33	0	9	0	9
H2-C3-O2-Fe27	34	0	5	0	5
H2-C4-Fe18	24	0	0	16	16
H2-C4-Fe23	29	0	99	214	313
H2-C4-O1-Fe22	29	0	0	4	4
H2-C4-O1-Fe26	33	0	1	0	1
H2-C4-O1-Fe27	34	0	5	0	5
H2-C4-O2-Fe21	29	0	0	5	5
H2-C5-Fe18	25	0	0	10	10
H2-C5-O2-Fe13	22	0	0	1	1
H2-C5-O2-Fe15	24	0	0	1	1
H2-C6-Fe16	24	0	0	15	15
H2-C6-O1-Fe13	22	0	2	5	7
H2-C6-O2-Fe12	22	0	2	0	2
H2-C6-O2-Fe17	27	0	0	1	1
H2-C7-Fe10	19	0	21	5	26
H2-C7-Fe13	22	0	99	258	357
H2-C7-Fe18	27	0	0	28	28
H2-C7-O1-Fe10	20	0	2	0	2
H2-C7-O1-Fe12	22	0	0	6	6
H2-C7-O2-Fe9	20	0	3	0	3
H2-C7-O2-Fe11	22	0	1	4	5
H2-C7-O2-Fe16	27	0	0	2	2
H2-C8-Fe10	20	0	68	6	74
H2-C8-O1-Fe9	20	0	1	1	2
H2-C8-O2-Fe8	20	0	2	0	2
H2-C9-Fe13	24	0	0	12	12
H2-C9-Fe16	27	0	0	10	10
H2-C9-O2-Fe15	28	0	1	0	1
H2-C10-Fe16	28	0	16	3	19
H2-C10-O1-Fe15	28	0	0	1	1
H2-C11-O1-Fe28	42	0	163	0	163
H2-C12-Fe28	42	0	55	0	55
H2-C12-Fe48	62	0	42	0	42
H2-C13-Fe30	45	0	49	0	49
H2-C13-O1-Fe28	44	0	268	0	268
H2-C14-Fe28	44	0	39	0	39
H2-C14-Fe33	49	0	43	0	43
H2-C20-Fe40	62	0	28	0	28
H2-C25-Fe35	62	0	89	0	89
H2-C30-Fe74	106	0	14	0	14

H2-C32-Fe74	108	0	60	0	60
H2-C32-O1-Fe74	109	0	47	0	47
H2-C42-Fe120	164	0	5	0	5
H2-C49-Fe96	147	0	21	0	21
H2-C49-Fe112	163	0	11	0	11
H2-C49-Fe120	171	0	12	0	12
H2-C50-Fe112	164	0	17	0	17
H2-C50-Fe120	172	0	13	0	13
H3-Fe26	29	0	4	0	4
H3-Fe29	32	0	0	1	1
H3-O2-Fe24	29	0	1	0	1
H3-C1-O1-Fe15	20	0	20	1	21
H3-C1-O1-Fe16	21	0	16	0	16
H3-C1-O1-Fe20	25	0	4	0	4
H3-C1-O2-Fe15	21	0	13	0	13
H3-C1-O2-Fe16	22	0	18	0	18
H3-C1-O2-Fe36	42	0	3	0	3
H3-C1-O3-Fe35	42	0	1	0	1
H3-C2-Fe22	27	0	0	13	13
H3-C2-Fe33	38	0	45	2	47
H3-C2-O2-Fe26	33	0	2	0	2
H3-C2-O2-Fe27	34	0	4	0	4
H3-C2-O3-Fe34	42	0	10	0	10
H3-C2-O3-Fe36	44	0	15	0	15
H3-C2-O4-Fe32	41	0	1	0	1
H3-C2-O4-Fe33	42	0	3	0	3
H3-C2-O4-Fe35	44	0	4	0	4
H3-C3-O1-Fe27	34	0	5	0	5
H3-C3-O2-Fe25	33	0	2	0	2
H3-C3-O3-Fe35	44	0	5	1	6
H3-C4-O2-Fe16	25	0	0	1	1
H3-C5-O1-Fe16	25	0	0	1	1
H3-C5-O2-Fe15	25	0	0	2	2
H3-C6-Fe16	25	0	102	226	328
H3-C6-Fe22	31	0	0	4	4
H3-C6-O1-Fe15	25	0	3	3	6
H3-C6-O2-Fe14	25	0	0	5	5
H3-C8-Fe14	25	0	0	6	6
H3-C12-O2-Fe36	53	0	157	0	157
H3-C13-Fe40	56	0	41	0	41
H3-C13-O2-Fe35	53	0	276	0	276
H3-C13-O2-Fe36	54	0	219	0	219
H3-C14-O2-Fe35	54	0	183	0	183
H3-C14-O2-Fe36	55	0	500	0	500

H3-C15-O1-Fe35	54	0	284	0	284
H3-C15-O1-Fe36	55	0	280	0	280
H3-C15-O2-Fe35	55	0	168	0	168
H3-C16-Fe35	54	0	134	0	134
H3-C16-Fe36	55	0	141	0	141
H3-C32-O1-Fe74	110	0	197	0	197
H3-C41-Fe120	164	0	6	0	6
H3-C49-Fe96	148	0	33	0	33
H3-C49-Fe112	164	0	5	0	5
H3-C49-Fe120	172	0	7	0	7
H3-C50-Fe120	173	0	20	0	20
H4-Fe12	16	232	0	13	245
H4-Fe17	21	0	0	12	12
H4-Fe20	24	0	4	0	4
H4-Fe24	28	0	2	0	2
H4-Fe32	36	0	26	0	26
H4-O1-Fe11	16	10	0	0	10
H4-O2-Fe10	16	8	0	0	8
H4-O2-Fe15	21	0	0	1	1
H4-O2-Fe18	24	0	1	0	1
H4-O2-Fe30	36	0	1	0	1
H4-C1-Fe31	36	0	99	2	101
H4-C1-Fe36	41	0	36	0	36
H4-C1-O1-Fe16	22	0	29	0	29
H4-C1-O1-Fe30	36	0	2	0	2
H4-C1-O1-Fe35	41	0	1	0	1
H4-C1-O2-Fe29	36	0	2	0	2
H4-C1-O2-Fe36	43	0	1	0	1
H4-C1-O3-Fe36	44	0	3	0	3
H4-C2-O1-Fe15	22	0	8	0	8
H4-C2-O2-Fe33	41	0	21	2	23
H4-C2-O3-Fe32	41	0	3	0	3
H4-C2-O3-Fe34	43	0	1	0	1
H4-C2-O4-Fe36	46	0	8	0	8
H4-C4	8	119	0	0	119
H4-C4-Fe16	24	0	0	15	15
H4-C4-O4-Fe36	48	0	0	2	2
H4-C5-O1-Fe14	24	0	0	1	1
H4-C6-Fe14	24	0	0	13	13
H4-C8-Fe46	58	0	15	1	16
H4-C8-O2-Fe30	44	0	48	0	48
H4-C9-O2-Fe26	41	0	53	0	53
H4-C9-O2-Fe27	42	0	36	0	36
H4-C10-O2-Fe30	46	0	19	0	19

H4-C11-O2-Fe23	40	0	1	0	1
H4-C11-O2-Fe27	44	0	46	0	46
H4-C11-O2-Fe29	46	0	39	0	39
H4-C12-Fe24	40	0	130	0	130
H4-C12-Fe28	44	0	50	0	50
H4-C12-Fe30	46	0	13	0	13
H4-C12-Fe34	50	0	40	0	40
H4-C12-Fe36	52	0	36	2	38
H4-C12-Fe40	56	0	48	2	50
H4-C12-Fe42	58	0	39	0	39
H4-C12-O1-Fe23	40	0	1	0	1
H4-C12-O1-Fe27	44	0	1	0	1
H4-C12-O2-Fe19	37	0	1	0	1
H4-C12-O2-Fe26	44	0	1	0	1
H4-C12-O2-Fe28	46	0	49	0	49
H4-C12-O2-Fe29	47	0	37	0	37
H4-C13-Fe20	37	0	26	0	26
H4-C13-O2-Fe19	38	0	1	0	1
H4-C13-O2-Fe25	44	0	1	0	1
H4-C14-Fe20	38	0	19	0	19
H4-C14-Fe26	44	0	53	2	55
H4-C14-Fe40	58	0	69	0	69
H4-C14-O1-Fe35	54	0	71	0	71
H4-C15-O2-Fe19	40	0	1	0	1
H4-C16-Fe19	39	0	22	0	22
H4-C16-Fe20	40	0	34	2	36
H4-C17-Fe19	40	0	42	0	42
H4-C17-Fe23	44	0	161	1	162
H4-C17-O1-Fe22	44	0	1	0	1
H4-C17-O2-Fe21	44	0	1	0	1
H4-C20-Fe31	55	0	12	5	17
H4-C20-Fe32	56	0	6	0	6
H4-C32-O1-Fe74	111	0	109	0	109
H4-C40-Fe16	60	0	63	0	63
H4-C50-Fe120	174	0	1	0	1
H4-C64-Fe148	216	0	4	0	4
H4-C64-O2-Fe148	218	0	1	0	1
H5-Fe16	21	0	10	0	10
H5-Fe27	32	0	2	0	2
H5-O2-Fe14	21	0	1	0	1
H5-C1-O2-Fe35	43	0	16	4	20
H5-C1-O3-Fe36	45	0	2	0	2
H5-C2-Fe21	28	0	0	11	11
H5-C2-Fe36	43	0	18	0	18

H5-C2-O2-Fe34	43	0	1	0	1
H5-C3-O2-Fe18	28	0	0	1	1
H5-C4-Fe19	28	0	0	33	33
H5-C6-Fe20	31	0	0	6	6
H5-C10-O1-Fe29	45	0	40	0	40
H5-C11-O1-Fe29	46	0	34	0	34
H5-C13-Fe35	53	0	151	0	151
H5-C14-Fe36	55	0	163	0	163
H5-C15-Fe20	40	0	24	0	24
H5-C15-Fe35	55	0	92	0	92
H5-C15-O1-Fe36	57	0	327	0	327
H5-C15-O2-Fe18	40	0	1	0	1
H5-C16-Fe36	57	0	119	0	119
H5-C32-Fe74	111	0	91	0	91
H5-C50-Fe120	175	0	6	0	6
H6-Fe10	16	0	0	24	24
H6-Fe15	21	0	9	0	9
H6-Fe16	22	0	87	82	169
H6-Fe25	31	0	54	130	184
H6-Fe26	32	15	8	11	34
H6-O1-Fe9	16	0	0	1	1
H6-O1-Fe14	21	0	1	0	1
H6-O1-Fe15	22	0	3	1	4
H6-O1-Fe24	31	0	3	4	7
H6-O1-Fe25	32	1	0	0	1
H6-O2-Fe14	22	0	2	3	5
H6-O2-Fe23	31	0	1	4	5
H6-O2-Fe24	32	0	0	1	1
H6-C1-O1-Fe33	41	0	7	0	7
H6-C1-O1-Fe35	43	0	7	0	7
H6-C1-O2-Fe36	45	0	1	0	1
H6-C1-O3-Fe36	46	0	4	0	4
H6-C2-Fe36	44	0	27	0	27
H6-C2-O2-Fe30	40	0	0	1	1
H6-C2-O2-Fe31	41	0	6	3	9
H6-C2-O2-Fe32	42	0	44	10	54
H6-C2-O2-Fe34	44	0	1	0	1
H6-C4	10	29	0	0	29
H6-C8-Fe48	62	0	22	0	22
H6-C12-Fe32	50	0	34	0	34
H6-C12-O1-Fe23	42	0	1	0	1
H6-C12-O1-Fe31	50	0	1	0	1
H6-C12-O2-Fe30	50	0	1	0	1
H6-C13-Fe23	42	0	66	0	66

H6-C13-O1-Fe22	42	0	1	0	1
H6-C13-O2-Fe21	42	0	2	0	2
H6-C14-O1-Fe35	56	0	149	0	149
H6-C16-O1-Fe27	50	0	2	0	2
H6-C17-Fe27	50	0	123	0	123
H6-C17-O2-Fe25	50	0	1	0	1
H6-C21-Fe35	62	0	62	0	62
H6-C26-O4-Fe72	108	0	3	0	3
H6-C28-O4-Fe72	110	0	2	0	2
H6-C32-Fe72	110	0	1	0	1
H7-Fe16	23	0	0	1	1
H7-Fe25	32	0	0	6	6
H7-O2-Fe23	32	0	0	1	1
H7-C1-O4-Fe34	46	0	1	1	2
H7-C2-Fe29	38	0	32	0	32
H7-C2-Fe35	44	0	11	0	11
H7-C2-Fe36	45	0	36	0	36
H7-C2-O2-Fe27	38	0	1	0	1
H7-C2-O2-Fe31	42	0	14	6	20
H7-C2-O2-Fe32	43	0	12	3	15
H7-C2-O2-Fe34	45	0	1	0	1
H7-C2-O2-Fe36	47	0	7	0	7
H7-C2-O5-Fe34	48	0	0	5	5
H7-C10-Fe36	53	0	77	0	77
H7-C14-Fe30	51	0	44	1	45
H7-C14-Fe35	56	0	314	0	314
H7-C15-Fe35	57	0	247	0	247
H7-C16-Fe34	57	0	39	0	39
H7-C23-Fe47	77	0	14	1	15
H8-Fe8	16	208	0	113	321
H8-Fe16	24	0	1	0	1
H8-Fe20	28	0	2	0	2
H8-O1-Fe7	16	9	0	5	14
H8-O2-Fe6	16	4	0	3	7
H8-C1-Fe27	36	0	70	1	71
H8-C1-O5-Fe36	50	0	1	1	2
H8-C2-O2-Fe32	44	0	3	1	4
H8-C2-O2-Fe36	48	0	4	0	4
H8-C2-O4-Fe34	48	0	5	1	6
H8-C2-O4-Fe35	49	0	2	0	2
H8-C2-O4-Fe36	50	0	7	0	7
H8-C3-O1-Fe36	48	0	6	0	6
H8-C7-Fe21	36	0	10	0	10
H8-C8-Fe42	58	0	25	0	25

H8-C12-O1-Fe23	44	0	1	0	1
H8-C13-Fe23	44	0	85	1	86
H8-C13-O1-Fe22	44	0	1	0	1
H8-C16-Fe38	62	0	37	0	37
H8-C19-Fe35	62	0	96	0	96
H8-C28-O2-Fe70	108	0	2	0	2
H9-Fe23	32	12	0	0	12
H9-C2-Fe16	27	0	2	0	2
H9-C2-O1-Fe34	46	0	1	0	1
H9-C2-O1-Fe35	47	0	0	2	2
H9-C2-O1-Fe36	48	0	7	0	7
H9-C3-O1-Fe35	48	0	3	0	3
H9-C12-Fe30	51	0	38	0	38
H9-C13-Fe17	39	0	28	1	29
H9-C16-O2-Fe23	50	0	2	0	2
H9-C17-Fe24	50	0	55	2	57
H9-C17-O1-Fe23	50	0	0	1	1
H9-C17-O2-Fe22	50	0	1	0	1
H9-C22-Fe46	77	0	7	2	9
H9-C30-Fe70	109	0	2	0	2
H10-Fe21	31	0	8	13	21
H10-Fe22	32	0	11	17	28
H10-O1-Fe20	31	0	0	1	1
H10-O1-Fe21	32	0	1	1	2
H10-C26-Fe70	106	0	1	0	1
H10-C28-Fe72	110	0	1	0	1
H10-C30-Fe70	110	0	2	0	2
H11-Fe5	16	0	1	87	88
H11-Fe16	27	0	0	1	1
H11-Fe21	32	0	0	14	14
H11-O1-Fe4	16	0	0	2	2
H11-O1-Fe20	32	0	0	1	1
H12-Fe19	31	0	0	40	40
H12-Fe32	44	0	26	1	27
H12-O2-Fe17	31	0	0	1	1
H12-C1-Fe31	44	0	105	1	106
H12-C1-O1-Fe30	44	0	1	0	1
H12-C1-O2-Fe29	44	0	3	0	3
H12-C4-O2-Fe19	37	0	1	0	1
H12-C5-Fe20	37	0	18	2	20
H12-C8-O2-Fe15	37	0	1	0	1
H12-C10-Fe15	37	0	18	0	18
H12-C10-O1-Fe14	37	0	3	0	3
H12-C15-Fe35	62	0	55	0	55

H12-C24-Fe39	75	0	22	0	22
H13-Fe16	29	0	167	221	388
H13-Fe19	32	0	0	5	5
H13-O1-Fe15	29	0	5	5	10
H13-O2-Fe14	29	0	1	7	8
H13-C2-Fe16	31	0	10	0	10
H13-C2-O1-Fe15	31	0	1	0	1
H13-C5-Fe22	40	0	6	0	6
H13-C17-Fe25	55	0	46	1	47
H14-Fe16	30	0	0	10	10
H14-Fe17	31	0	0	8	8
H14-Fe18	32	0	0	8	8
H14-O2-Fe14	30	0	0	1	1
H14-O2-Fe20	36	0	0	1	1
H14-C1-Fe21	36	0	0	14	14
H14-C1-O2-Fe19	36	0	0	1	1
H14-C2-Fe20	36	0	0	36	36
H14-C2-Fe40	56	0	1	0	1
H14-C2-O2-Fe18	36	0	0	2	2
H15-Fe6	21	0	33	0	33
H15-Fe16	31	0	0	9	9
H15-Fe17	32	0	0	19	19
H15-O1-Fe5	21	0	1	0	1
H15-O1-Fe15	31	0	0	1	1
H15-O1-Fe16	32	0	0	2	2
H15-C1-Fe16	32	0	0	5	5
H15-C1-O2-Fe20	38	0	0	1	1
H15-C2-Fe21	38	0	0	17	17
H15-C2-O2-Fe19	38	0	0	1	1
H15-C4-Fe19	38	0	0	24	24
H15-C4-O2-Fe17	38	0	0	1	1
H15-C9-O2-Fe14	40	0	1	0	1
H15-C11-Fe14	40	0	40	1	41
H15-C11-O2-Fe12	40	0	1	1	2
H16-Fe5	21	0	44	1	45
H16-Fe16	32	0	1	44	45
H16-O1-Fe15	32	0	0	1	1
H16-O2-Fe3	21	0	2	0	2
H16-O2-Fe14	32	0	0	5	5
H16-C2-Fe16	34	0	21	0	21
H16-C2-Fe20	38	0	26	0	26
H16-C2-O1-Fe15	34	0	1	0	1
H16-C2-O1-Fe19	38	0	1	0	1
H16-C4-Fe20	40	0	10	0	10

H16-C4-O2-Fe18	40	0	1	0	1
H17-Fe15	32	0	0	9	9
H17-C1-Fe26	44	0	51	0	51
H17-C1-O1-Fe25	44	0	1	0	1
H17-C1-O2-Fe24	44	0	3	0	3
H17-C2-Fe16	35	0	19	0	19
H17-C2-O1-Fe20	40	0	1	0	1
H17-C2-O2-Fe14	35	0	1	0	1
H17-C3-Fe20	40	0	15	0	15
H17-C4-Fe21	42	0	0	24	24
H17-C5-Fe24	46	0	7	0	7
H18-Fe13	31	0	0	4	4
H18-C1-Fe11	30	0	74	18	92
H18-C1-Fe21	40	0	0	30	30
H18-C1-O1-Fe10	30	0	3	1	4
H18-C1-O2-Fe9	30	0	0	1	1
H18-C2-Fe16	36	0	30	0	30
H18-C2-Fe20	40	0	19	0	19
H18-C2-Fe26	46	0	4	0	4
H18-C2-O1-Fe15	36	0	1	0	1
H18-C2-O2-Fe14	36	0	1	0	1
H19-Fe12	31	0	145	3	148
H19-Fe13	32	0	0	3	3
H19-Fe21	40	0	0	19	19
H19-O1-Fe11	31	0	6	0	6
H19-O2-Fe10	31	0	4	0	4
H19-C2-Fe20	41	0	8	0	8
H19-C2-Fe21	42	0	0	16	16
H19-C2-O2-Fe19	42	0	0	1	1
H20-C2-Fe67	89	0	1	0	1
H23-Fe8	31	0	10	4	14
H23-Fe9	32	0	15	8	23
H23-O1-Fe7	31	0	1	0	1
H23-O1-Fe8	32	0	1	0	1
H24-Fe8	32	0	0	2	2
H24-C2-Fe20	46	0	34	0	34
H24-C2-O1-Fe19	46	0	2	0	2
H24-C2-O2-Fe18	46	0	1	0	1
H26-C2-Fe40	68	0	6	0	6
H27-C2-Fe35	64	0	17	0	17
H27-C2-Fe36	65	0	21	0	21
H27-C2-Fe58	87	0	0	3	3
H29-C2-Fe39	70	0	2	0	2
H33-C2-Fe40	75	0	7	0	7

H34-C6-Fe40	80	0	2	0	2
H34-C10-Fe48	92	0	1	0	1
H35-C2-Fe30	67	0	1	0	1
H37-C2-Fe30	69	0	1	0	1
H38-C2-Fe45	85	0	3	0	3
H40-C2-Fe45	87	0	2	0	2
H41-C2-Fe39	82	0	18	0	18
H42-C2-Fe40	84	0	36	0	36
H44-C2-Fe39	85	0	2	0	2
H45-C2-Fe40	87	0	33	2	35
H46-C2-Fe40	88	0	5	0	5
H47-C2-Fe40	89	0	26	0	26
H48-C2-Fe40	90	0	4	0	4
H50-C2-Fe48	100	0	4	0	4
H52-C2-Fe48	102	0	5	0	5
total	--	675	15093	5644	21412

2. Benchmark of G-NN potential against DFT calculations

Table S2. Benchmark of NN calculations for FeC_x systems as compared with DFT results. Listed data includes the compositions, total atom number per cell (N_{atom}), DFT energy, NN energy and energy differences between DFT energy and NN energy (E_{diff} , meV/atom).

Composition	N _{atom}	E _{DFT} (eV/cell)	E _{NN} (eV/cell)	E _{diff} (meV/atom)
bulk				
Fe12C4_1	16	-135.04	-134.95	-6.09
Fe12C4_2	16	-134.82	-134.88	3.74
Fe12C4_3	16	-134.89	-134.90	1.13
Fe12C4_4	16	-134.98	-134.93	-3.15
Fe12C4_5	16	-134.84	-134.85	0.93
Fe16C8_1	24	-204.44	-204.43	-0.58
Fe16C8_2	24	-204.36	-204.39	1.53
Fe16C8_3	24	-204.37	-204.39	0.97
Fe16C8_4	24	-204.23	-204.27	1.61
Fe16C8_5	24	-204.12	-204.20	3.50
Fe20C8_1	28	-237.27	-237.26	-0.56
Fe20C8_2	28	-237.20	-237.08	-4.11
Fe20C8_3	28	-237.15	-237.13	-0.74
Fe20C8_4	28	-237.13	-237.12	-0.29
Fe20C8_5	28	-237.08	-237.09	0.33
Fe24C6_1	30	-251.13	-251.19	2.11
Fe24C6_2	30	-251.22	-251.19	-0.88
Fe24C6_3	30	-251.14	-251.12	-0.67
Fe24C6_4	30	-251.14	-251.11	-0.82
Fe24C6_5	30	-251.07	-251.12	1.61
Fe22C10_1	32	-271.86	-271.86	-0.03
Fe22C10_2	32	-271.82	-271.81	-0.26
Fe22C10_3	32	-271.92	-271.83	-2.91
Fe22C10_4	32	-271.73	-271.75	0.39
Fe22C10_5	32	-271.81	-271.76	-1.60
Fe20C12_1	32	-272.03	-272.05	0.60
Fe20C12_2	32	-271.97	-271.96	-0.14
Fe20C12_3	32	-271.97	-271.97	-0.12
Fe20C12_4	32	-271.97	-271.96	-0.22
Fe28C12_1	40	-339.43	-339.33	-2.57
Fe28C12_2	40	-339.40	-339.29	-2.81
Fe28C12_3	40	-339.37	-339.27	-2.44
Fe28C12_4	40	-339.34	-339.27	-1.86
Fe28C12_5	40	-339.35	-339.27	-2.02
Fe24C16_1	40	-339.60	-339.70	2.56
Fe24C16_2	40	-339.60	-339.70	2.52
Fe24C16_3	40	-339.62	-339.62	-0.04

Fe24C16_4	40	-339.49	-339.62	3.33
Fe44C20_1	64	-543.63	-543.50	-1.97
Fe44C20_2	64	-543.62	-543.59	-0.59
Fe44C20_3	64	-543.61	-543.52	-1.37
Fe44C20_4	64	-543.61	-543.63	0.31
Fe44C20_5	64	-543.55	-543.44	-1.74
surface				
θ -Fe ₃ C(010)	44	-367.05	-367.11	-1.32
χ -Fe ₅ C ₂ (100)	40	-334.21	-334.18	0.62
χ -Fe ₅ C ₂ (510)	58	-477.43	-477.40	0.63
χ -Fe ₅ C ₂ (111)	50	-413.85	-414.15	-5.99
α -Fe ₇ C ₃ -II(010)	40	-334.19	-334.16	0.93
η -Fe ₂ C(011)	24	-199.15	-199.02	5.46
η -Fe ₂ C(110)	22	-183.22	-183.34	-5.15
η -Fe ₂ C(111)	31	-257.64	-257.64	0.23

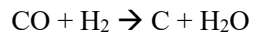
* Mean error between DFT energy and NN energy is 2.28 meV/atom.

Table S3. Comparision of the energetics for H and CO adsorption on $\theta\text{-Fe}_3\text{C}(010)$, $\chi\text{-Fe}_5\text{C}_2(100)$, $\chi\text{-Fe}_5\text{C}_2(510)$, $\chi\text{-Fe}_5\text{C}_2(111)$, $\text{o-Fe}_7\text{C}_3\text{-II}(010)$, $\eta\text{-Fe}_2\text{C}(011)$, $\eta\text{-Fe}_2\text{C}(110)$ and $\eta\text{-Fe}_2\text{C}(111)$, and CO activation on $\chi\text{-Fe}_5\text{C}_2(510)$ from G-NN and DFT calculations. The listed data includes the adsorption free energy G_{ad} of H and CO and the CO dissociation barrier through a carbon vacancy formation G_a .

	Surface	G-NN	VASP	Diff
$G_{\text{ad}}(\text{H}_{\text{Fe-site}})$	$\theta\text{-Fe}_3\text{C}(010)$	0.30	0.18	-0.12
	$\chi\text{-Fe}_5\text{C}_2(100)$	0.29	0.15	-0.13
	$\chi\text{-Fe}_5\text{C}_2(510)$	-0.22	-0.38	-0.16
	$\chi\text{-Fe}_5\text{C}_2(111)$	0.00	-0.18	-0.18
	$\text{o-Fe}_7\text{C}_3\text{-II}(010)$	0.29	0.16	-0.13
	$\eta\text{-Fe}_2\text{C}(011)$	0.23	0.15	-0.08
	$\eta\text{-Fe}_2\text{C}(110)$	0.69	0.48	-0.21
	$\eta\text{-Fe}_2\text{C}(111)$	-0.25	-0.35	-0.09
$G_{\text{ad}}(\text{H}_{\text{C-site}})$	$\theta\text{-Fe}_3\text{C}(010)$	0.28	0.20	-0.09
	$\chi\text{-Fe}_5\text{C}_2(100)$	0.30	0.20	-0.10
	$\chi\text{-Fe}_5\text{C}_2(510)$	0.01	-0.10	-0.11
	$\chi\text{-Fe}_5\text{C}_2(111)$	-0.07	-0.34	-0.27
	$\text{o-Fe}_7\text{C}_3\text{-II}(010)$	0.30	0.21	-0.09
	$\eta\text{-Fe}_2\text{C}(011)$	0.31	0.34	0.02
	$\eta\text{-Fe}_2\text{C}(110)$	-0.12	-0.35	-0.23
	$\eta\text{-Fe}_2\text{C}(111)$	0.09	-0.05	-0.14
$G_{\text{ad}}(\text{CO})$	$\theta\text{-Fe}_3\text{C} (010)$	-0.56	-0.65	-0.09
	$\chi\text{-Fe}_5\text{C}_2 (100)$	-0.57	-0.66	-0.10
	$\chi\text{-Fe}_5\text{C}_2 (510)$	-0.53	-0.70	-0.17
	$\chi\text{-Fe}_5\text{C}_2 (111)$	-1.07	-1.06	0.01
	$\text{o-Fe}_7\text{C}_3\text{-II}(010)$	-0.70	-0.66	0.04
	$\eta\text{-Fe}_2\text{C}(011)$	-0.54	-0.57	-0.03
	$\eta\text{-Fe}_2\text{C}(110)$	-0.50	-0.67	-0.18
	$\eta\text{-Fe}_2\text{C}(111)$	-0.81	-0.79	0.02
$G_a(\text{CO(V)} \rightarrow \text{C+O})$	$\chi\text{-Fe}_5\text{C}_2(510)$	1.29	1.11	-0.18

3. Calculations of carbon chemical potential (μ_C)

The carbon chemical potential (μ_C) is determined from the equilibrium among typical FTS reactants/products (CO, H₂, C₂H₄ and H₂O). For example, for Eq.2 in the main text:



$$\mu_C = \mu_{\text{CO}} + \mu_{\text{H}_2} - \mu_{\text{H}_2\text{O}} - E_C$$

where E_C is the DFT energy of a free carbon atom and μ_{CO} , μ_{H_2} and $\mu_{\text{H}_2\text{O}}$ are chemical potentials for CO, H₂ and H₂O gas phases. Chemical potential for gas phase is calculated as follows:

$$\mu(T, P) = E(\text{DFT}) + ZPE + \Delta H(0 \rightarrow 298 \text{ K}, P_0) + \Delta H(298 \text{ K} \rightarrow T, P_0) - TS(T, P_0) + k_B T \ln \frac{P}{P_0} \quad (4)$$

where enthalpy (H) and entropy (S) terms are taken from the standard thermodynamics data in NIST Chemistry WebBook and NIST-JANAF Thermochemical Tables.

Table S4. Energetics of iron carbide bulk phases.

	ZPE (eV/f.u.)	ΔG_f ($\mu_C = -6.60 \text{ eV}$, eV/C)	ΔG_f ($\mu_C = -6.90 \text{ eV}$, eV/C)	ΔG_f ($\mu_C = -7.20 \text{ eV}$, eV/C)	ΔG_f ($\mu_C = -7.43 \text{ eV}$, eV/C)
Fe ₄ C	0.25	-0.56	-0.26	0.04	0.27
θ -Fe ₃ C	0.21	-0.75	-0.45	-0.15	0.08
χ -Fe ₅ C ₂	0.39	-0.81	-0.51	-0.21	0.02
α -Fe ₇ C ₃ -II	0.58	-0.82	-0.52	-0.22	0.01
Fe _{2.2} C	0.20	-0.82	-0.52	-0.22	0.01
η -Fe ₂ C	0.19	-0.84	-0.54	-0.24	-0.01
Fe ₅ C ₃	0.53	-0.73	-0.43	-0.13	0.10
Fe ₃ C ₂	0.34	-0.68	-0.38	-0.08	0.15
α -Fe ₇ C ₃	0.54	-0.82	-0.52	-0.22	0.01
h-Fe ₇ C ₃	0.56	-0.75	-0.45	-0.15	0.08
Fe_bcc	0.04	--	--	--	--

Table S5. Fe₇C₃ bulk phase energy calculated by DFT+U where U value is set to be +3 eV for 3d states of Fe.

	DFT+U (eV/f.u.)
α -Fe ₇ C ₃ -II	-66.58 (0)
α -Fe ₇ C ₃	-66.36 (+0.22)
h-Fe ₇ C ₃	-66.21 (+0.37)

4. FeC_x bulk phases

Figure S1. Structure of Fe₄C GM. Fe: orange, C: grey.

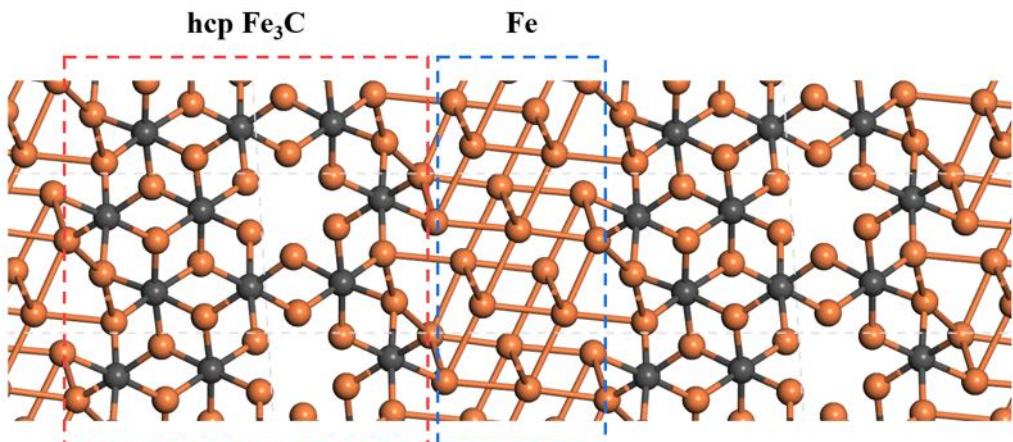
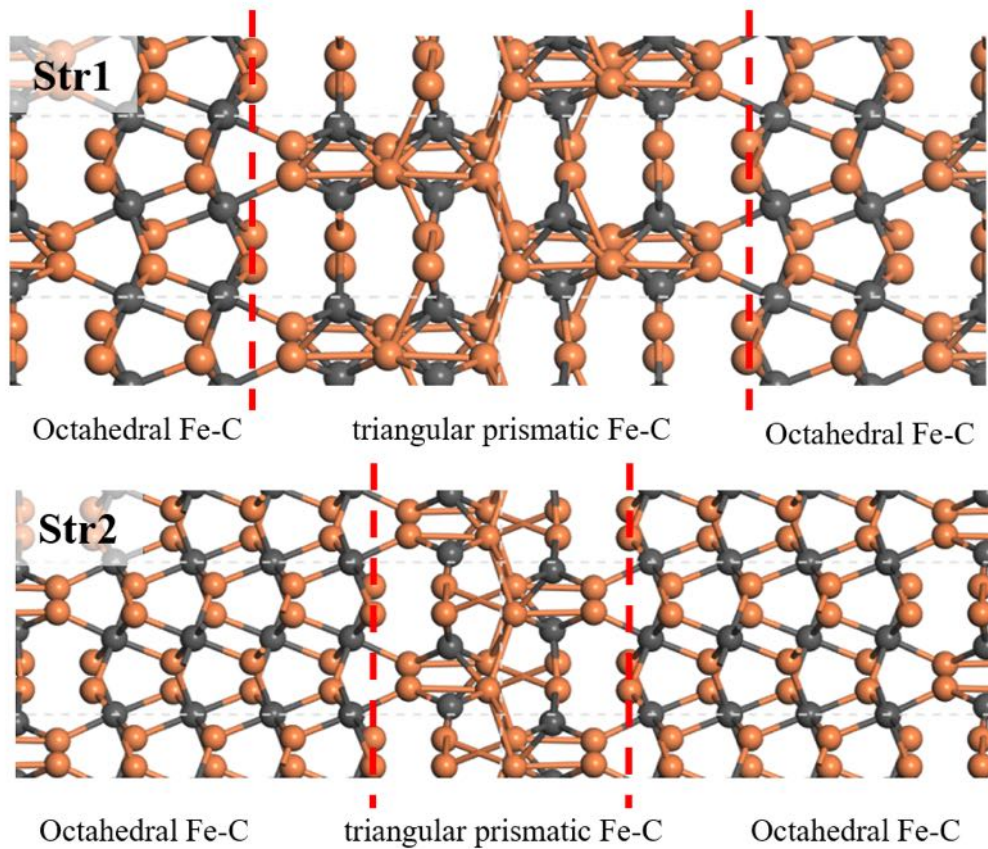


Figure S2. Phases with mixed octahedral and triangular prismatic Fe-C coordinations labelled in Fe₇C₃ PES (Str1 and Str2). Fe: orange, C: grey.



5. FeC_x surfaces

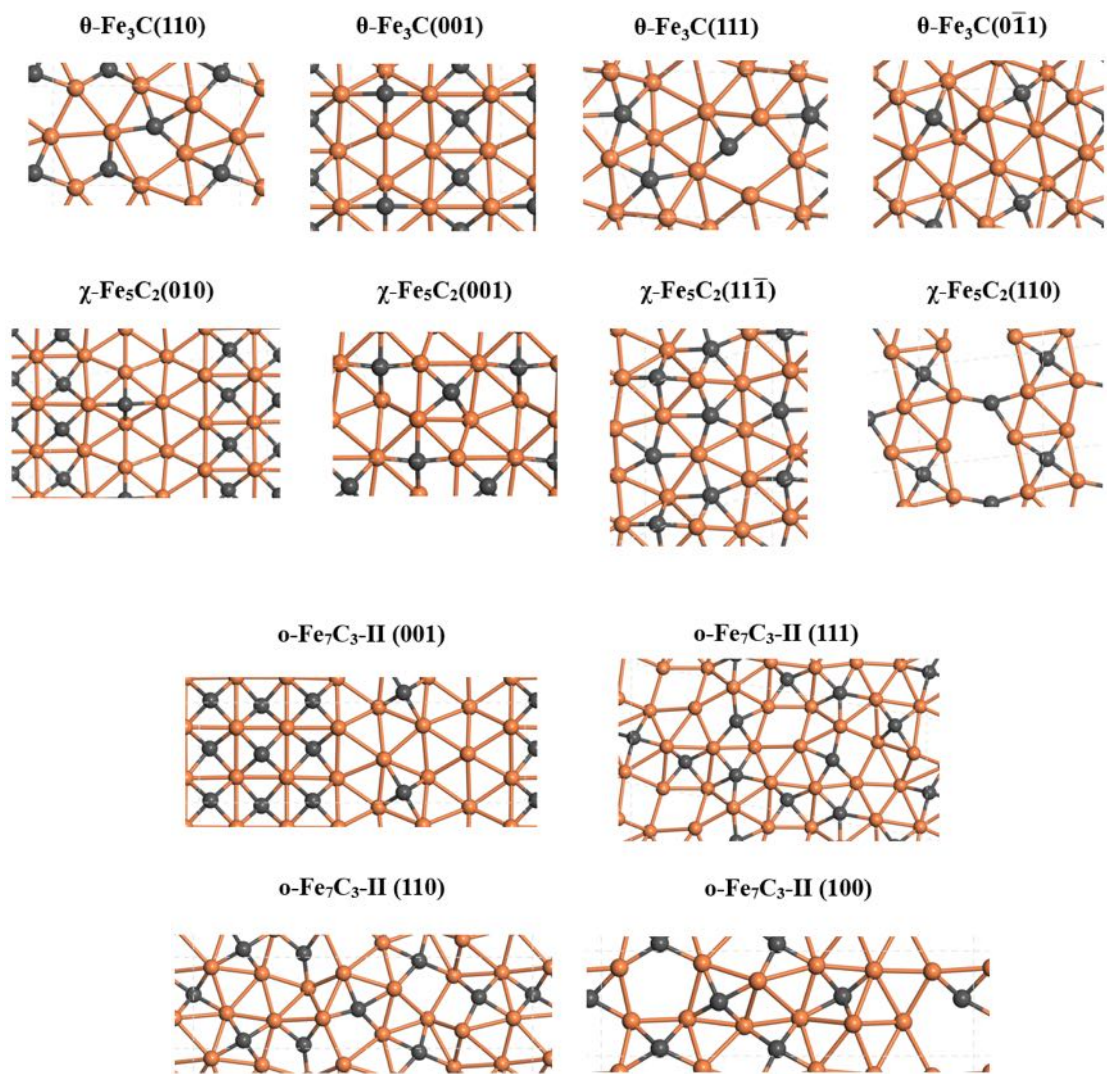
Table S6. All the surfaces investigated in this work.

Surface	surface free energy γ (J/m ²)		Fe/C ratio
	$\mu_C = -6.90$ eV	$\mu_C = -7.20$ eV	
θ -Fe ₃ C			
θ-Fe₃C(010)	1.50	1.64	2.00
θ -Fe ₃ C(110)*	2.01	2.14	2.00
θ -Fe ₃ C(001)*	2.01	2.16	2.00
θ -Fe ₃ C(111)	2.17	2.20	3.00
θ -Fe ₃ C(0-11)	2.27	2.27	4.00
χ -Fe ₅ C ₂			
χ-Fe₅C₂(100)	1.68	1.77	2.00
χ -Fe ₅ C ₂ (510)*	1.75	1.83	2.00
χ -Fe ₅ C ₂ (111)	1.81	1.95	1.75
χ -Fe ₅ C ₂ (010)*	2.03	2.11	2.00
χ -Fe ₅ C ₂ (11-1)*	2.11	2.24	1.75
χ -Fe ₅ C ₂ (001)	2.37	2.37	2.50
χ -Fe ₅ C ₂ (110)*	2.41	2.41	2.00
α -Fe ₇ C ₃ -II			
α-Fe₇C₃-II(010)*	1.88	1.88	2.00
α -Fe ₇ C ₃ -II(001)*	2.07	2.13	2.00
α -Fe ₇ C ₃ -II(111)	2.32	2.43	2.50
α -Fe ₇ C ₃ -II(110)	2.52	2.67	2.33
α -Fe ₇ C ₃ -II(100)*	2.61	2.61	2.40
α -Fe ₇ C ₃			
α -Fe ₇ C ₃ (101)*	1.95	2.01	2.29
α -Fe ₇ C ₃ (100)	1.96	2.06	2.33
α -Fe ₇ C ₃ (001)	2.21	2.21	2.50
α -Fe ₇ C ₃ (111)	2.23	2.23	3.00
α -Fe ₇ C ₃ (011)	2.25	2.25	2.50
α -Fe ₇ C ₃ (010)	2.32	2.35	2.00
η -Fe ₂ C			
η-Fe₂C(011)	1.72	1.72	2.00
η-Fe₂C(110)	1.76	1.89	1.50
η-Fe₂C(111)*	1.83	1.92	2.00
η -Fe ₂ C(101)*	2.07	2.07	2.00
η -Fe ₂ C(100)	2.33	2.33	2.00
η -Fe ₂ C(010)	2.45	2.61	1.00
η -Fe ₂ C(001)	2.46	2.46	2.00

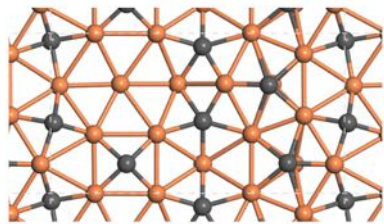
The asterisk indicates the surface is reconstructed.

The surface free energy for the surfaces of θ -Fe₃C still refers to its own bulk phase, although the bulk is no longer a convex point at $\mu_C = -7.20$ eV.

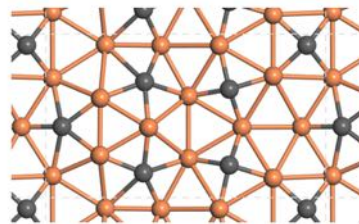
Figure S3. The other surfaces in our work. Fe: orange, C: grey.



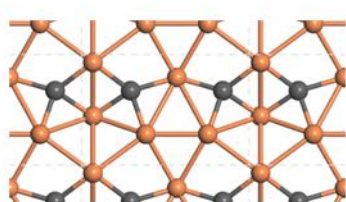
$\text{o-Fe}_7\text{C}_3(101)$



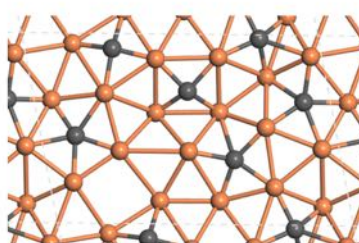
$\text{o-Fe}_7\text{C}_3(100)$



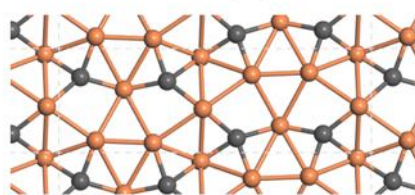
$\text{o-Fe}_7\text{C}_3(001)$



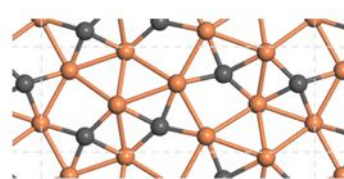
$\text{o-Fe}_7\text{C}_3(111)$



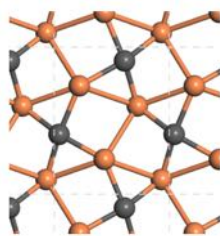
$\text{o-Fe}_7\text{C}_3(011)$



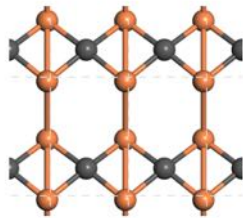
$\text{o-Fe}_7\text{C}_3(010)$



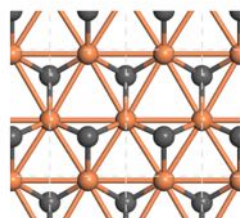
$\eta\text{-Fe}_2\text{C}(101)$



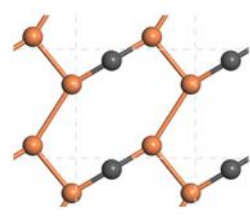
$\eta\text{-Fe}_2\text{C}(100)$



$\eta\text{-Fe}_2\text{C}(010)$



$\eta\text{-Fe}_2\text{C}(001)$



6. Adsorption sites for H/CO

Table S7. The most stable H/CO adsorption geometry for eight stable surfaces, corresponding to the adsorption free energy in Table 1. Fe: orange, C: grey, H: white, O: red.

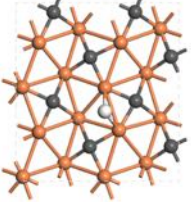
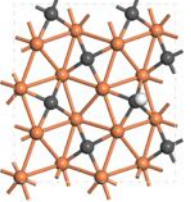
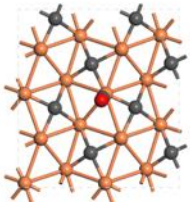
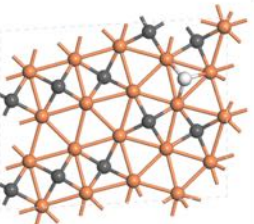
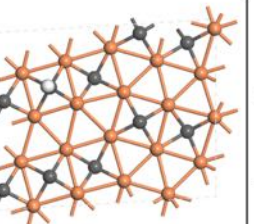
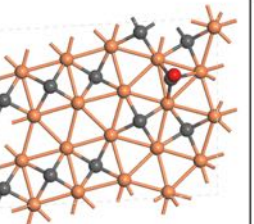
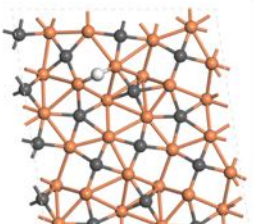
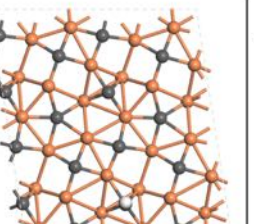
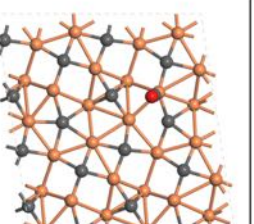
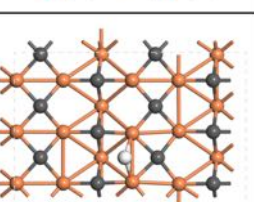
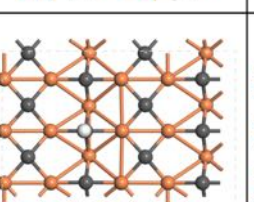
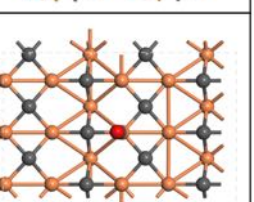
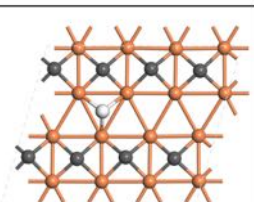
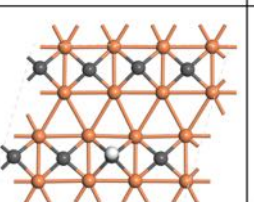
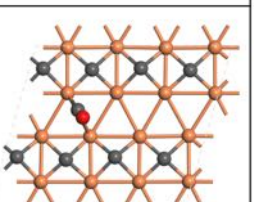
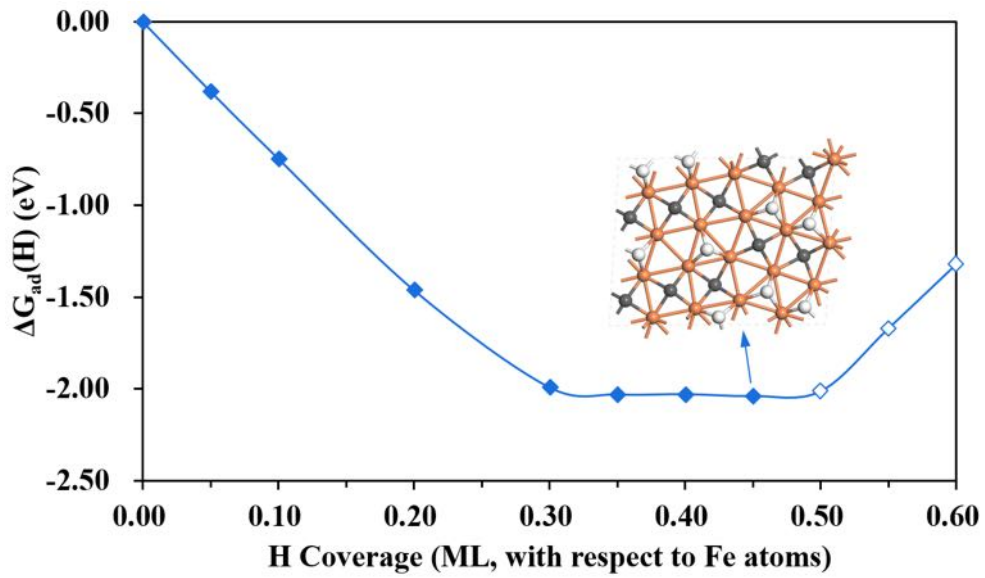
Surface	H adsorption site		CO adsorption site
	Fe-H	C-H	
$\theta\text{-Fe}_3\text{C}(010)$ $\chi\text{-Fe}_5\text{C}_2(100)$ $\sigma\text{-Fe}_7\text{C}_3\text{-II}(010)$ $\eta\text{-Fe}_2\text{C}(011)$			
$\chi\text{-Fe}_5\text{C}_2(510)$			
$\chi\text{-Fe}_5\text{C}_2(111)$			
$\eta\text{-Fe}_2\text{C}(110)$			
$\eta\text{-Fe}_2\text{C}(111)$			

Figure S4. The total Gibbs free energy for H adsorption on $\chi\text{-Fe}_5\text{C}_2$ (510) at T=523 K, P(H₂)=1.67 MPa with an increase of H coverage on the surface. The maximum H coverage on $\chi\text{-Fe}_5\text{C}_2$ (510) is 0.45 ML with respect to surface Fe atoms (0.90 ML with respect to surface C atoms). Fe: orange, C: grey, H: white.



7. H and C diffusion on the surface from molecular dynamics

Figure S5. The temperature and the conserved quantity (system energy) at 523 K on $\gamma\text{-Fe}_5\text{C}_2(510)$ in the 5 ns simulation.

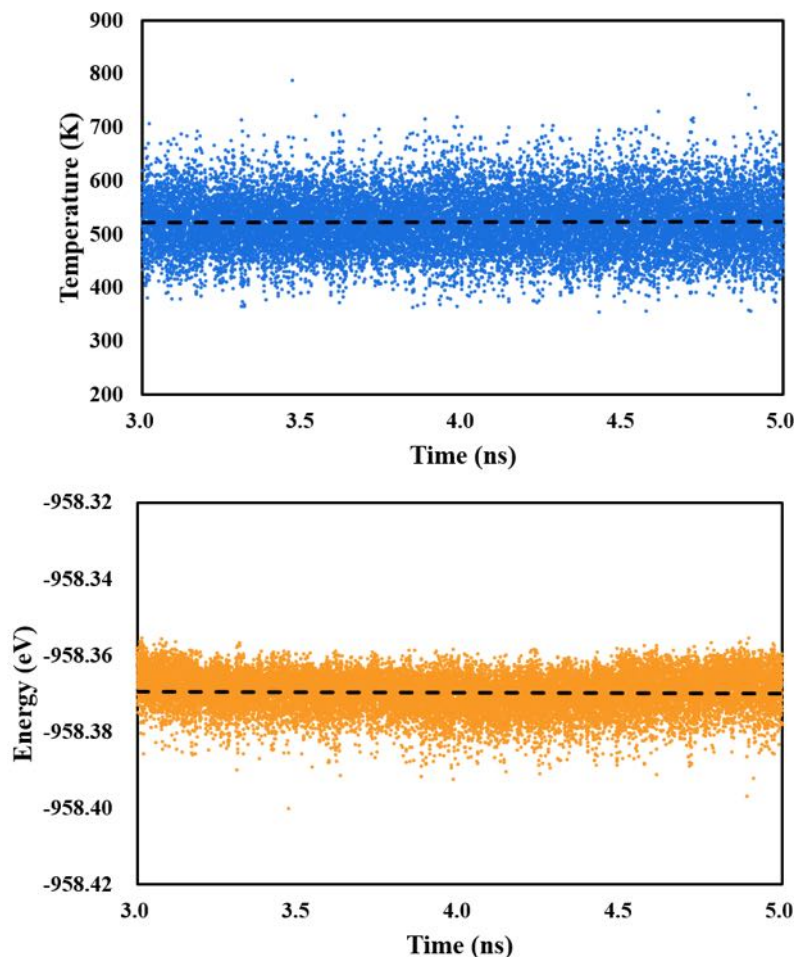
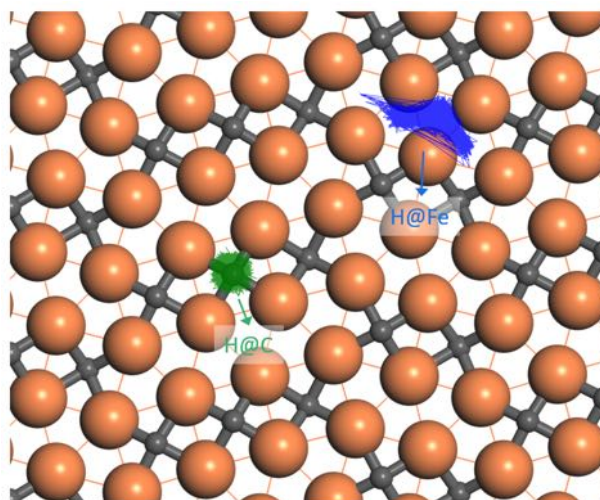


Figure S6. The diffusion trajectory for H at 523 K on $\gamma\text{-Fe}_5\text{C}_2(510)$ collected from the final 2 ns snapshots in the 5 ns simulation. The H on Fe sites (H@Fe) has a larger diffusion area (blue line) while H on C site (H@C) is trapped (green line). Fe: orange, C: grey.



8. Other CO activation pathways and CH_x diffusion pathway

Figure S7. The vibrational frequencies of the TS (left) and the extrapolation from TS to IS and FS (right) for CO dissociation (TS3 in the main text) on $\gamma\text{-Fe}_5\text{C}_2$ (510). Fe: orange, C: grey, O: red.

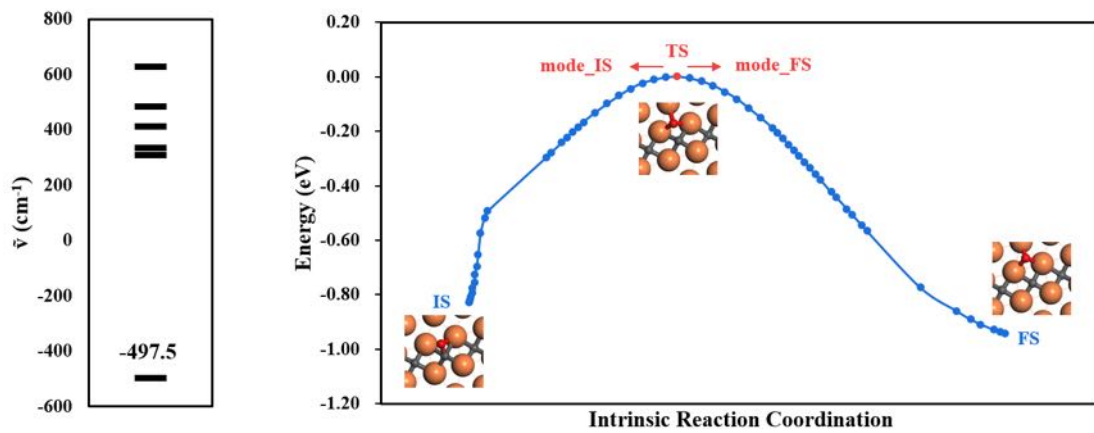


Figure S8. Reaction energy profiles of direct CO dissociation on Fe sites, C-assisted CO dissociation via CCO and H-assisted CO dissociation via CHO and CH₂O pathways at T=523K, P=2.5 MPa, H₂/CO= 2/1 on γ -Fe₅C₂ (510). The formation pathway of COH and CHO species are also shown in dotted line. The overall barriers for the formation of CHO, COH, CH₂O and CHOH species are 1.59, 1.95, 2.16 and 2.58 eV, respectively. The overall barriers for the direct CO dissociation, C-assisted CO dissociation via CCO and H-assisted CO dissociation via CHO and CH₂O are 2.64, 2.44, 2.24 and 2.41 eV, respectively. The asterisk indicates the adsorption state. The structure snapshots for the reaction intermediates and TS are also shown. Fe: orange, C: grey, H: white, O: red.

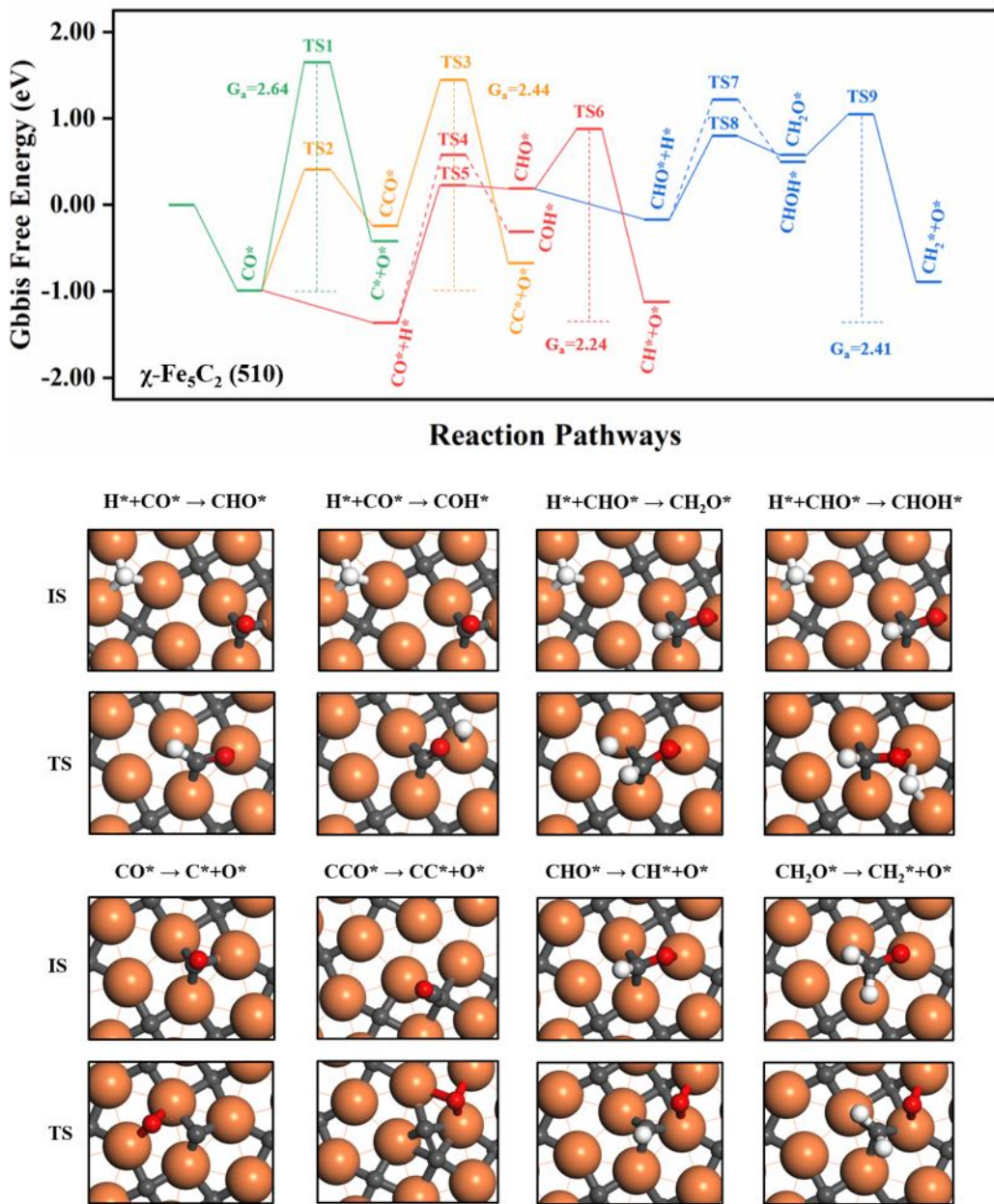
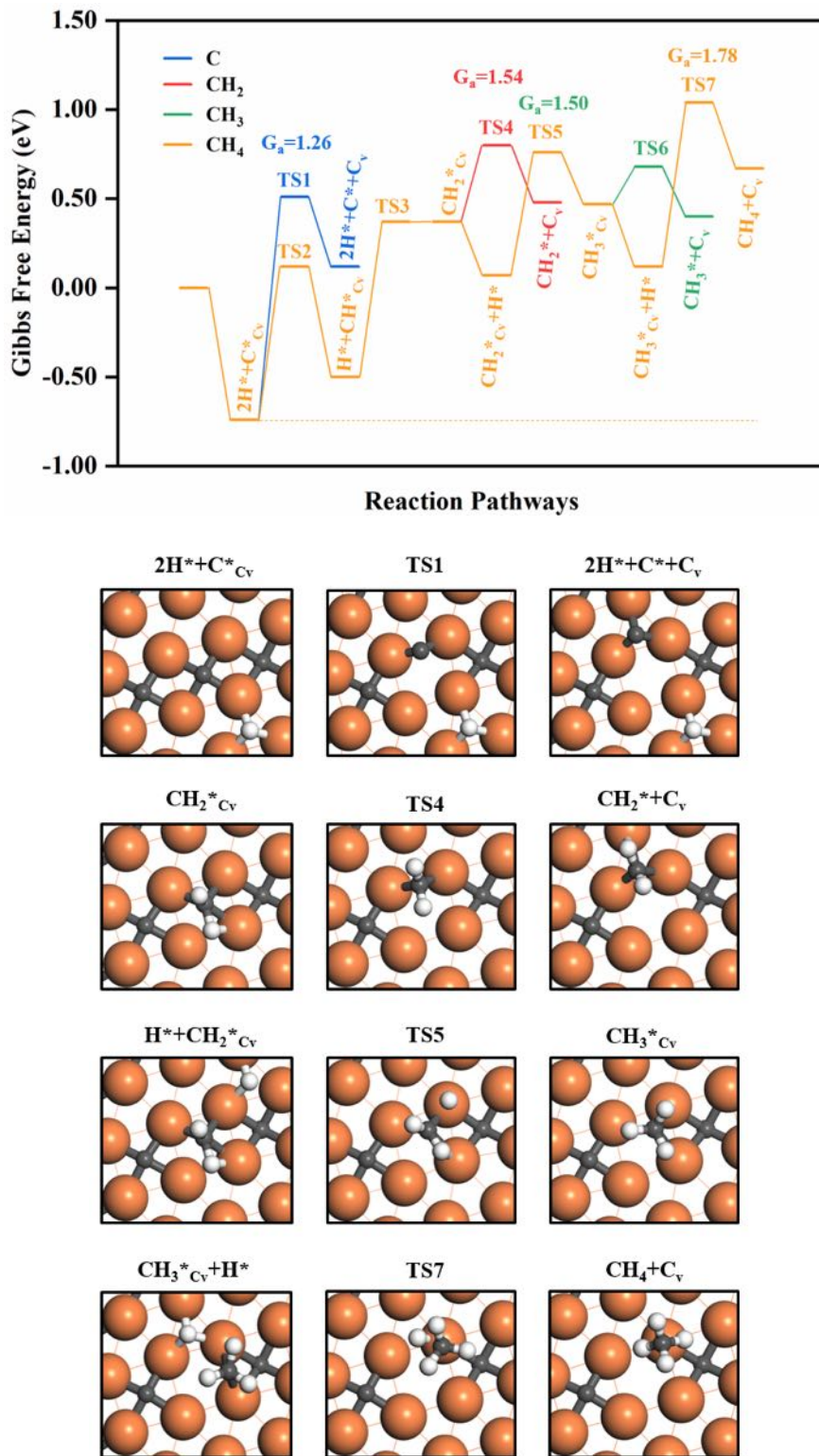


Figure S9. Reaction energy profile for the formation of C vacancy via CH_x ($x=0, 2, 3, 4$) species at $T=523\text{K}$, $P=2.5\text{ MPa}$, $\text{H}_2/\text{CO}=2/1$ on $\gamma\text{-Fe}_3\text{C}_2$ (510). The asterisk indicates the adsorption state. C_v denotes the C-vacancy site. Fe: orange, C: grey, H: white, O: red. The overall barriers for the formation of C vacancy through the diffusion of C, CH_2 and CH_3 and CH_4 are 1.26, 1.54, 1.50 and 1.78 eV, respectively. Fe: orange, C: grey, H: white.



Reference:

- (1) Huang, S.-D.; Shang, C.; Zhang, X.-J.; Liu, Z.-P. Material Discovery by Combining Stochastic Surface Walking Global Optimization with a Neural Network. *Chem. Sci.* **2017**, *8*, 6327-6337.
- (2) Huang, S.-D.; Shang, C.; Kang, P.-L.; Liu, Z.-P. Atomic Structure of Boron Resolved Using Machine Learning and Global Sampling. *Chem. Sci.* **2018**, *9*, 8644-8655.
- (3) Behler, J.; Parrinello, M. Generalized Neural-network Representation of High-dimensional Potential-energy Surfaces. *Phys. Rev. Lett.* **2007**, *98*, 146401.
- (4) Behler, J. Representing Potential Energy Surfaces by High-dimensional Neural Network Potentials. *J. Phys. Condens. Mat.* **2014**, *26*, 183001.
- (5) Shang, C.; Liu, Z.-P. Stochastic Surface Walking Method for Structure Prediction and Pathway Searching. *J. Chem. Theory Comput.* **2013**, *9*, 1838-1845.
- (6) Zhang, X.-J.; Shang, C.; Liu, Z.-P. From Atoms to Fullerene: Stochastic Surface Walking Solution for Automated Structure Prediction of Complex Material. *J. Chem. Theory Comput.* **2013**, *9*, 3252-3260.
- (7) Shang, C.; Zhang, X.-J.; Liu, Z.-P. Stochastic Surface Walking Method for Crystal Structure and Phase Transition Pathway Prediction. *Phys. Chem. Chem. Phys.* **2014**, *16*, 17845-17856.